UC San Diego
UC San Diego Previously Published Works

Title

The Argo: a high channel count recording system for neural recording in vivo

Permalink

https://escholarship.org/uc/item/5911p4v1

Journal

Journal of Neural Engineering, 18(1)

ISSN

1741-2560

Authors

Sahasrabuddhe, Kunal
Khan, Aamir A
Singh, Aditya P
et al.

Publication Date

2021-02-01

DOI

10.1088/1741-2552/abd0ce

Peer reviewed

The Argo: A high channel count recording system for neural recording *in vivo*

Kunal Sahasrabuddhe[1], **Aamir A. Khan**[1], **Aditya P. Singh**[1], **Tyler M. Stern**[1], **Yeena Ng**[1], **Aleksandar Tadi**[1], **Peter Orel**[1], **Chris LaReau**[1], **Daniel Pouzzner**[1], **Kurtis Nishimura**[1], **Kevin M. Boergens**[1], **Sashank Shivakumar**[1], **Matthew S. Hopper**[1], **Bryan Kerr**[1], **Mina-Elraheb S. Hanna**[1], **Robert J. Edgington**[1], **Ingrid McNamara**[1], **Devin Fell**[1], **Peng Gao**[2], **Amir Babaie-Fishani**[2], **Sampsa Veijalainen**[2], **Alexander V. Klekachev**[2], **Alison M. Stuckey**[1], **Bert Luyssaert**[2], **Takashi D. Y. Kozai**[3,4,5,6,7], **Chong Xie**[8,9,10], **Vikash Gilja**[11], **Bart Dierickx**[2], **Yifan Kong**[1], **Malgorzata Straka**[1], **Harbaljit S. Sohal**[1], **Matthew R. Angle**[1]

[1]Paradromics, Inc, Austin, TX, USA

[2]Caeleste CVBA, Mechelen, Belgium

[3]Department of Bioengineering, University of Pittsburgh, Pittsburgh, PA, USA

[4]Center for the Neural Basis of Cognition, University of Pittsburgh, Pittsburgh, PA, USA

[5]McGowan Institute of Regenerative Medicine, University of Pittsburgh, Pittsburgh, PA, USA

[6]Center for Neuroscience, University of Pittsburgh, Pittsburgh, PA, USA

[7]NeuroTech Center, University of Pittsburgh Brain Institute, Pittsburgh, PA, USA

[8]Department of Electrical and Computer Engineering, Rice University, Houston, TX, USA

[9]Department of Bioengineering, Rice University, Houston, TX, USA

[10]NeuroEngineering Initiative, Rice University, Houston, TX, USA

[11]Department of Electrical and Computer Engineering, University of California, San Diego, La Jolla, CA, USA

Abstract

Objective.—Decoding neural activity has been limited by the lack of tools available to record from large numbers of neurons across multiple cortical regions simultaneously with high temporal fidelity. To this end, we developed the Argo system to record cortical neural activity at high data rates.

Approach.—Here we demonstrate a massively parallel neural recording system based on platinum-iridium microwire electrode arrays bonded to a CMOS voltage amplifier array. The Argo system is the highest channel count in vivo neural recording system, supporting simultaneous

---

recording from 65,536 channels, sampled at 32 kHz and 12-bit resolution. This system was designed for cortical recordings, compatible with both penetrating and surface microelectrodes.

Main results.—We validated this system through initial bench testing to determine specific gain and noise characteristics of bonded microwires, followed by *in-vivo* experiments in both rat and sheep cortex. We recorded spiking activity from 791 neurons in rats and surface LFP activity from over 30,000 channels in sheep.

Significance.—These are the largest channel count microwire-based recordings in both rat and sheep. While currently adapted for head-fixed recording, the microwire-CMOS architecture is well suited for clinical translation. Thus, this demonstration helps pave the way for a future high data rate intracortical implant.

Keywords

microelectrode array; microwires; auditory cortex; brain-computer interface; electrophysiology; sheep; rats

Introduction:

Motor and sensory information are represented in the brain by coordinated ensembles of neurons with topographic maps that can span several centimeters in large animals and humans. Decoding information from these representations necessarily requires recording from large numbers of individual neurons with high temporal fidelity [1]. As a result, there has been a recent impetus in both experimental and translational neuroscience to record from more neurons [2–5].

Within the field of experimental neuroscience, there have been significant advances in both electrical and optical methods for recording from large populations of neurons, each having its respective advantages. Optical methods for recording neural activity have made major strides through the development of fluorescent proteins such as genetically encoded calcium indicators (e.g. GCaMP6/7[6,7]) and voltage sensitive fluorescent proteins (e.g. Archon [8] or QuasAR [8,9]). These new fluorescent probes enable functional imaging experiments that can simultaneously record from as many as 10,000 neurons in vivo [2,8,9]. While these are powerful experimental tools, approaches based on fluorescent proteins face significant barriers in clinical translation and can only record from shallow regions of the brain without implantable optics. Further, the expression of exogenous fluorescent proteins requires modification of host cells, which has substantial safety and regulatory implications when applied to humans. Lastly, the scattering of light in the brain and thermal sensitivity of brain tissue creates significant engineering challenges for developing a practically implantable imaging system that can spatially resolve activity without overheating tissue [10,11].

By contrast, electrical recording is well established as a tool for basic science and clinical research [12]. Intracortical electrode arrays are used for brain-computer interface applications [13–17] and intraoperative recording [18–20]. The state of the art in clinical neurophysiology, the Utah Array [13,21], Blackrock Microsystems, USA), has enabled several notable applications in neural prosthetics [14,17,22], despite having a limited electrode count (100 electrodes) and covering only a small 4 mm × 4 mm cortical area.

Success with the Utah Array has motivated efforts to record from more neurons over larger areas of the brain. The main approach has been the insertion of multiple Utah arrays in a single patient [15,17], but the low density of electrodes and lack of multiplexing in the Utah array make the technology difficult to scale to higher channel counts.

Many recent efforts to 'scale up' neurophysiology have focused on lithographically patterned, thin film-based probes. Most notable are those based on active CMOS probes (e.g. Neuropixel [3]) and flexible thin-films stacks (e.g. Polyimide + metal [4,23]). These high channel-count devices have enabled novel experimental paradigms with acute and semi-chronic recording, but they have yet to be demonstrated as robust for chronic implantation in large animals. Thin silicon probes are fragile, and polymer-substrate probes commonly suffer from cracking [24] and delamination between insulation and electrode [25,26].

One technological approach that is both highly scalable and promises more immediate clinical application is the use of microwire-CMOS arrays [5,27]. These devices use arrays of parallel microwire electrodes, which are connected to active CMOS electronics for readout and stimulation. Microwire electrodes consist of a conductive metal wire core insulated by a solution-resistant dielectric such as a polymer or ceramic. Microwires have been used consistently and reliably over the last 70 years to record extracellular action potentials from the brains of experimental animal models and humans [28–31]. They are highly robust and suitable for chronic applications [28–31] and translational models [18,32–34]. Importantly, recent work with carbon-fiber based probes suggests that the foreign body response to inserted microwires can be dramatically reduced by using wires with diameters less than 20 μm [35–37].

Traditionally, microwire technology has been less scalable than integrated silicon probes due to the difficulty of connecting large arrays to a large number of amplifiers [30,31,38]. Recently, however, simultaneous, parallel bonding of microwire arrays to high density CMOS sensor arrays have been successfully demonstrated [5], paving the way for large format arrays of many thousands of wires that would not otherwise be achievable.

To date, demonstrations of the microwire-CMOS concept have involved adapting CMOS arrays that were not specifically designed for the application and have limited channel count due to restrictions in the array readout [5]. To fully realize the potential of microwire-CMOS technology, we have designed a custom CMOS application-specific integrated circuit (ASIC), electronics, firmware, and software, providing an end-to-end solution for large scale recording.

This "Argo system" represents a significant advance in total data throughput, simultaneously addressing up to 65,536 channels at 32 kHz and 12 bits of resolution. The CMOS readout array can be bonded to microwire electrode arrays of varying electrode length, count, and spacing, creating a highly versatile system applicable to different experimental models. It is designed for recording in a head-fixed, in vivo preparation. Full sensor readout produces a data rate of up to 26 Gbps, which can be simultaneously streamed directly to disk and viewed in real-time through a web browser-based digital oscilloscope interface. To validate our system, we performed initial recordings in the rat cortex with arrays of up to 1300

penetrating microwires, detecting action potentials from 791 single-units. To demonstrate the large channel count recording capability of the device, we performed surface recording of stimulus-evoked local field potentials from the sheep auditory cortex with a microwire-based electrocorticography array with over 30,000 channels.

Methods:

System overview

The Argo system is designed to enable simultaneous data acquisition on up to 65,536 channels at sampling rates of 32 kHz [39]. The system consists of an array of platinum-iridium (PtIr) microwire electrodes, a custom CMOS voltage-amplifier array designed to read and amplify neural signals [5,27], electronics to process and packetize these signals, and a computer that runs the custom data acquisition software and user interface server (Figure 1). Individual components are described in detail in subsequent sections.

Microwire Arrays for Neural Recording

The recording array consists of a stochastically ordered array of microwires (Tanaka Kikinzoku International, Japan) compressively and reversibly bonded to a custom CMOS amplifier array. The microwire cores are platinum-iridium alloy (90% Pt/10% Ir), selected for their biocompatibility and demonstrated recording/stimulation performance *in vivo* [40,41].

The fabrication process for our microwire arrays has been described previously [5]. For intracortical arrays, the distal ends of the microwire electrodes are electro-sharpened in a parallel process adapted from [5,42,43]. Microwires were bonded to a printed circuit board used to short all microwires and deliver electrical signals to them, and their distal ends were dipped in a 0.5 M $CaCl_2$ solution. Sharp tips were formed by controlling the voltage applied to the wires in solution, and the speed at which wires were drawn out of solution. The amplitude, frequency, pulse duration, and duty cycle of the voltage applied to the wires were modulated using a Chroma Programmable AC Source (Model 61603, Chroma ATE, Taiwan). The wire speed was controlled using a stepper motor (ZST225B, ThorLabs, USA) and stepper motor controller (KST1, ThorLabs, USA), wires could be sharpened to arbitrary taper lengths and tip angles. The wire sharpening process consisted of four steps: (1) wire length equalization, (2) coarse electrosharpening, (3) fine electrosharpening, and (4) electrochemical polishing of the wire tips.(See Supplementary Table S1 for system parameters, and Supplementary Table S2 for sharpening process parameters). Between steps, the solution is circulated through a large bath using a preristaltic pump (Model 07528–10, Cole Parmer, USA) to evacuate reaction products. The final tip diameter is smaller than 200 nm (Figure 2A) to alleviate the "bed-of-nails", or dimpling, effect that is commonly associated with the implantation of high density electrode arrays (<400 μm pitch) into cortical tissue [44,45]. Non-penetrating electrode arrays do not require this sharpening step, therefore tip preparation is performed later in the process.

Microwires are then insulated with a thick sacrificial parylene-C layer to set the electrode spacing (100–400 μm). Following the coating step, the wires are tightly packed into a

fluorinated ethylene propylene (FEP) heat shrink tube that is then shrunk to fix the wire positions within the array. Next, the proximal end of the array is prepared to ensure good electrical contact with the CMOS array when the array is mechanically pressed against the face of the sensor array [5]. This is achieved by polishing the proximal end of the array to be flat and then exposing the microwires at the proximal ends 10–20 μm by ashing in oxygen plasma using an SPI Plasma Prep III system (SPI Supplies, USA).

For non-penetrating electrode arrays, the tips are prepared by polishing the entire distal end of the array at this stage. This ensures that the recording sites are co-planar, smooth, and appropriately exposed.

For penetrating electrodes, the shank lengths of the distal ends (tips) of the bundled microwires are defined by ashing them with oxygen plasma as described above. At this stage, the arrays are coated with a robust 20–30 nm Atomic Layer-Deposited (ALD) alumina coating (Savannah S200, Cambridge NanoTech, MA, USA) to provide a high-quality insulation layer [46] that is then selectively de-insulated to define the length of the recording site at the wire tip. Recording sites have a typical impedance of around 300–500 kΩ at 1 kHz in physiological saline. The electrode-tissue interface is approximated by the equivalent Randles circuit [47] that is commonly used to model results from electrochemical impedance spectra for tungsten microwires [48] and platinum microelectrode arrays [49,50]. In this circuit, the electrolyte (tissue or saline bath) is modeled as a resistor, in series with the interface itself, which is modeled as a parallel combination of the double-layer capacitance and the faradaic impedance [47]. In the spiking band, both capacitive and resistive elements contribute to the interface impedance [40].

We developed smaller arrays of between 100 and 1300 electrosharpened electrodes for *in vivo* experiments in rats, with the number of electrodes increasing as our array development advanced. The larger arrays prepared with flat tips for Local Field Potential (LFP) recordings in sheep had over 30,000 electrodes. All arrays were stochastically ordered due to the fabrication process used. The reference electrode was 80 μm diameter teflon (PTFE)-coated PtIr wire (AM Systems, USA) that was de-insulated 1–2 mm from one end and placed in subdural space. The other end of the wire was connected to a gold pin (Mill-Max, USA) that was inserted into a receptacle on the front-end board (see Methods: Argo System Electronics) during characterization and *in vivo* recording experiments.

CMOS Sensor Design

The sensor in the Argo system is an application-specific integrated circuit (ASIC) designed to amplify and filter neural signals from a high-density microwire array. It was co-designed by Paradromics and Caeleste, CVBA (Belgium) and fabricated by X-FAB Silicon Foundries (Germany and Malaysia) in a 180 nm CMOS process technology node. The sensor consists of a pixel array of 256×256 pixels with a pixel pitch and dimensions of 50 μm $\times$ 50 μm, adding up to an active area of 12.8 mm $\times$ 12.8 mm for the readout array. The peripheral circuit elements for control and readout increase the total dimensions of the ASIC to 14.5 mm $\times$ 16 mm.

Each pixel has a 40 μm × 40 μm top metal pad which is used as the landing pad for the microwire electrode. This top metal pad is AC-coupled to a low-noise amplifier (LNA) chain. The LNA chain is composed of three main blocks: input amplifiers, an antialiasing low-pass filter, and an output column buffer (Figure 3).

The amplifiers are implemented as common-source gain stages that are biased to operate in the class A regime. This topology was chosen due to its good linear response, high input impedance, and low noise. The drawbacks are higher power consumption and lower gain. To limit the power consumption and at the same time achieve the required gain of 100 V/V, the design implements two amplifiers in series, with each amplifier contributing a gain of approximately 10 V/V. In addition, each amplifier has a tunable input biasing circuit which in conjunction with an AC coupling input capacitor forms a tunable high-pass filter. Thus, the amplifier block provides a cascaded second order high-pass filter that has its 3dB point tunable from approximately 18 Hz to 300 Hz. This serves two functions. The first is the removal of DC offsets, drifts, and slowly varying out-of-band high amplitude signals. These undesired signal components can saturate the input and diminish the signal dynamic range, ultimately reducing the ability of the system to acquire meaningful signals. The second is to provide the flexibility of the system to operate in two modes. In one mode, setting the corner frequency to 18 Hz enables both neuron spiking activity and LFP to be recorded, since the latter has most of its integrated power below 100 Hz. In the second mode, LFP signals can be rejected by increasing the corner to higher frequencies. This allows for spiking signals to retain the entire dynamic range. The amplifier is designed to have a high input impedance to ensure that signals are not attenuated by the voltage divider formed by the electrode-tissue interface and the amplifier. Specifically, the input impedance of the amplifier at 1 kHz has a resistive component of 4.4 GΩ and a capacitive component of 0.4 GΩ (400 fF). This ensures that the amplifier can accommodate a variety of electrodes with up to 10 MΩ impedance at 1 kHz for future applications, well above the 300 – 500 kΩ impedances seen for our electrodes (see Discussion: Future Recording Applications).

To keep the integrated noise floor as low as possible while simultaneously providing antialiasing, the amplifier chain is followed by a third order low-pass filter with a tunable corner frequency between 8 kHz and 50 kHz. In our application all three corners are set to 20 kHz resulting in a 3dB point at approximately 12 kHz and providing 6.78 dB of signal suppression at the Nyquist frequency of 16 kHz.

The output buffer of the pixel provides isolation between the pixel output and the column line used to multiplex the pixels in a single column. That is, when one of the pixels in the column is being read out the other pixels have their outputs disconnected from the line to avoid overloading. This reduces crosstalk between pixels and ensures that each pixel can read out signals from unique electrodes.

In the ASIC periphery, a set of control circuits and high-bandwidth amplifiers convert the multiplexed signal from single-ended to differential and bring the total gain of the signal chain to around 800 V/V. The sensor multiplexes 2048 individual channels to each of 32 high-speed analog outputs from the entire array. Furthermore, the output buffers are

designed to drive long transmission lines leading to the external analog-to-digital converters ADCs.

Argo Power Supply

The Argo system can be powered using a 6V battery (LC-R0612P1 Panasonic, Japan) with a 5V regulator or using a power supply (72–2710 Tenma, Japan) with galvanic isolation from the environment. The choice of which to use was based on noise measurements made prior to recording, with the power supply preferred as long as noise levels were $< 10\ \mu V_{RMS}$. For rat surgeries, we found that using the power supply resulted in acceptable noise levels ($< 10\ \mu V_{RMS}$) during recording. For the sheep surgeries, the noise floor remained outside this range when using the power supply, likely due to additional equipment such as the ventilator and other surgical equipment that were not present in rat surgeries. Using the battery, however, noise levels were found to be $< 10\ \mu V_{RMS}$, so all recordings in sheep were performed using the battery to power the Argo system.

Argo System Electronics

The system electronics consist of two custom printed circuit boards (PCBs). The first PCB (front-end board) is designed to house the CMOS sensor and support electronics. The second PCB (main board) is designed to digitize analog signals and deliver them to the server (Figure 4). It is designed in a rigid-flex form factor for the reasons of signal integrity, compactness, and ease of assembly.

The CMOS sensor is wire-bonded to the front-end board, which also contains a reference connector and a set of precision voltage regulators for the sensor. The front-end board is mounted in a metal housing designed to reliably connect with the microwire array after pressing (see Methods: Array connectivity testing for more details) [27].

The main board contains two 16-channel high-speed ADCs (ADS52J90, Texas Instruments, USA) as well as a Field-Programmable Gate Array (FPGA, XC7K160T-2FFG676–2, Xilinx, USA). The headstage requires an external 5V/3A DC power source and is kept galvanically isolated from powerline and other electronic noise sources, which can otherwise corrupt neural signals. The main board is housed within a separate headstage body designed to connect with the front-end main board frame. Electrical connections between the two boards are made via high-density spring-loaded pins, shown in Figure 4(D)) (855–22-040–30-001101, Mill-Max, USA). This allows reliable and repeatable mating between the boards without imposing extreme tolerance constraints on the fabrication of either the boards or the mechanical components. Two banks of pins transmit the multiplexed, high-speed analog output signals from the CMOS sensor to the ADCs (Figure 4(E)), while the third separate bank of pins transmits control signals from the FPGA to the CMOS sensor.

The ADC's input signal range of 2 Vpp translates to an input signal range of ~2.6 mVpp in the CMOS amplifiers, given the 763 V/V average gain (see Methods: CMOS Sensor Design). The ADCs operate at a sampling frequency of 78.125 MHz, corresponding to a sensor sampling rate of 32 kHz, and digitize the analog signal to a 12-bit digital signal that is then transmitted to the FPGA over tightly impedance-controlled Low-Voltage Differential Signalling (LVDS) pairs. This high sampling rate provides further protection from aliasing

artifacts. It also allows for spike sorting applications of the neural data, wherein a higher sampling rate leads to better cluster/unit separability in PCA space for an individual spiking channel [51,52].

The FPGA (Figure 4(G)) then demultiplexes the wide-band digitized signals from the 32 LVDS channels into the original 65,536 channels and remaps them to construct a 256 × 256pixel raster at 32 kHz. The logic in the FPGA generates timing signals for raster scanning the 256×256 pixels CMOS sensor array at a rate of up to 32,000 frames per second.

The FPGA is also used to coordinate data transfer to the host computer via a 40 gigabit Ethernet link through an OM3 optical fiber (943–99684-10005, Amphenol, USA). As the physical layer of the 40GBASE-SR4 protocol, the FPGA drives a Quad Small Form-factor Pluggable (QSFP+) optical transceiver (Figure 4(H)) through its 8 GTX transceivers. An embedded application processor (Xilinx Microblaze) within the FPGA fabric coordinates the ARP, ICMP, and UDP communication for control signals to and from the host computer. In order to maintain throughput for the high-speed neural data, the FPGA fabric directly assembles UDP packets using header information set by the embedded processor.

Computer systems for neural readout and data storage

To handle the large amount of data generated by the Argo system, the host computer is custom-built on a Supermicro dual Xeon server platform (X10DAC, Supermicro, USA) running Ubuntu Linux 18.04 Server Edition and equipped with two Intel Xeon E5–2640 v4 processors, 64 GB of ECC RAM and an Intel XL710 network interface card for 40GBASE-SR4 communication with the Argo headstage. This host server runs a fully custom data acquisition software package. This software produces two data streams: one raw data stream to be written to disk, and another stream to be served externally through a websockets interface, where data can be accessed through the application programming interface (API). The data acquisition software package is built on Intel's Data Plane Development Kit (DPDK) to ingest the raw ethernet packets at full 40 Gbps line rate. The packets are evaluated for checksum integrity at the application level and are rearranged to be written to an array of 20 hard drives using Direct Memory Access (DMA) and a custom multi-threaded sharding system.

High-performance computing technologies such as core pinning, cache line optimization, and memory alignment are used throughout the data acquisition software stack to enable recording of full frame neural data at full 32 kHz frame rate. This allows the user to record data continuously for up to 8 hours, the duration of a typical acute sheep experiment, without running out of disk space or needing multiple recording systems in the surgical environment.

Both recording and export functions within the software were written to be fault-tolerant. If a hard disk were to fail during recording, the software would write data to the remaining drives, and if it were to fail immediately after an experiment, the export function would ensure lost data would not be included in the analysis.

User interface for live data visualization

A custom UI for real-time monitoring was developed for the Argo system to facilitate in-experiment data validation required for collection of high-quality datasets. Some salient features of the UI include customizable bandpass filters (e.g. 300–6000 Hz for recording in the spike band), powerline filters (50/60 Hz), common average referencing [53] across all or a selected subset of channels and the ability to listen to channels of interest. These features were used to ensure that denoising was performed appropriately prior to the experiment and to determine whether data collected was electrophysiological in nature.

By default, the UI is initialized with a raster image of the sensor, producing a spatial map of activity on all channels. This enables the user to implement connectivity masks (see Methods: Array connectivity testing for more detail). Each pixel on the raster represents an individual amplifier channel, and each channel's raw or filtered output can be viewed in a separate trace-scope, in either live-stream mode, or in threshold-trigger mode, similar to an oscilloscope.

The UI server also has an API that can be used to control the system through an external program such as MATLAB to facilitate additional analyses (e.g. channel RMS values or power spectrum plots) during recording sessions.

Array connectivity testing

To complete the assembly of the device, microelectrode arrays were physically pressed [5] onto the chip while monitoring connectivity. The press mechanism allows electrode arrays to be physically bonded to the CMOS sensor in a reversible and reliable manner. This approach was preferable to permanent fixation (e.g. using glue or epoxy) as it allowed for re-use of both the electrode arrays and the CMOS chip.

The connectivity was assessed in the physiological saline bath by submerging electrode recording sites while applying a 2 kHz, > 2mV$_{PP}$ sine wave. Using the UI described previously, the pressed array was adjusted until maximal connectivity was observed and the press was stabilized with set screws on the housing within the front-end board. This completed the process of bonding the microwire electrode array to the CMOS sensor.

Next, a quantitative connectivity test was performed to determine the gain and noise of the electrically coupled array-chip device. Gain and noise were calculated using a custom MATLAB program (MATLAB 2018a, Mathworks, USA) that fetches data through the system API described previously. The gain on every pixel was calculated by applying a 2 kHz, 0.5 mV peak to peak sine wave signal in the saline bath and measuring the recorded voltage. The noise was then calculated by shorting the system reference to the saline bath (with no external signal applied). The noise measurement was band-pass filtered between 300 Hz and 6 kHz (i.e., within the spiking band). The input-referred noise was determined using the recorded root mean squared (RMS) noise values and the gain for each pixel calculated in the previous step.

The connectivity map was determined using *k*-means clustering of gain and noise values. Clusters with appropriate gain (mean > 650 V/V) and noise (mean <10 μV$_{RMS}$) were

considered optimally connected to the system, with the number of clusters set interactively by the user to achieve these thresholds. From this analysis, a connectivity mask was generated to remove unconnected channels from subsequent analysis.

Animal Surgery

Rat Surgery—This study and all experimental protocols were approved by the Institutional Animal Care and Use Committee (IACUC) at the University of Texas at Austin, which follows the National Institutes of Health (NIH) guidelines for the ethical treatment of animals. Male Sprague Dawley rats (Charles River, 250–400 g) were used for implanting Argo microwire arrays. Rodents were housed in a laboratory environment on a 12-h light and dark cycle at 25°C, with *ad libitum* access to food and water.

Animals were anesthetized in an induction chamber on 3% isoflurane and then transferred to a small animal stereotaxic frame (Narishige, Japan) and maintained at 2.5% isoflurane for the duration of the procedure. Hair was removed from the head with small animal shears, Puralube (Dechra, UK) was placed on the eyes, and the surgical sites were sterilized with alternating povidone-iodine and alcohol pads prior to incision. Temperature was monitored rectally, and a heat mat was placed under the animal for the duration of the procedure with temperature maintained at around 36.0–36.5°C.

An incision was made through the scalp exposing the skull. The fascia was reflected and the periosteum was removed from the bone. A small craniotomy was made (5×5 mm) with a microdrill (OmniDrill 35, World Precision Instruments, USA) and the margins were removed with rat skull-appropriate bone rongeurs to extend the craniotomy to accommodate a 10 mm diameter microwire array. A durotomy was then performed with the use of microscissors. Once the durotomy was completed a micromanipulator was used to insert the Argo Microwire array into the brain and physiological saline was applied to keep the brain moist during the experiment. Argo microwires were inserted 0.7–1 mm into the brain to ensure that most of the electrodes would reside in the grey matter of the brain to enable recording of neural unit activity. A schematic of the experimental setup is shown in Figure 5.

To create a reference electrode, an 80 μm diameter teflon (PTFE)-coated PtIr wire (AM Systems, USA) was de-insulated 1–2 mm from one end. The deinsulated end was then placed in the subdural space. The wire was secured in place with gel foam (Pfizer, USA) and secured on the skull with the application of UV-curable dental acrylic (Flowable Composite 101–6773, Henry Schein, USA). This limited the motion of the reference wire to reduce the possibility of picking up microphonic noise.

Sheep Surgery—This study and all experimental protocols were approved by the Institutional Animal Care and Use Committee (IACUC) at the Bridge PTS, San Antonio, Texas, which follows the National Institute of Health (NIH) guidelines for the ethical treatment of animals. White face Dorset Sheep (Ovis aries) that weighed 30 to 35 kg were used for this study. Food was withheld for 24 hours prior to surgery, while water was provided to the sheep *ad libitum*.

For sheep, anesthesia induction was achieved by using an IM injection of Tiletamine/ Zolazepam (Telazol, 4–6 mg/kg). The sheep was intubated, and anesthesia was maintained via 1–5% isoflurane delivered in 60% oxygen and 40% medical grade air. An orogastric tube was placed to minimize or prevent ruminal bloat. Ophthalmic ointment (Paralube, Dechra, UK) was applied to prevent corneal desiccation. Thermal support was provided via a circulating warm water blanket (T/Pump, Stryker, USA) during the course of anesthesia or Bair hugger (3M, USA).

Once the sterile field was prepared, an incision was made over the skull to expose the bone and underlying fascia. The tissue was reflected, and the periosteum removed over the exposed skull. Next, a surgical microdrill (OmniDrill 35, World Precision Instruments, USA) was used to perform the craniotomy. Bone rongeurs were used to remove excess bone and fully expose the surface of the dura. A craniotomy was made (typically 3×3 cm) over the auditory cortex in the sheep. Typical stereotaxic coordinates were 5 mm anterior and 25–30 mm medial from bregma point for the center point of the craniotomy. After the craniotomy, a durotomy was performed to expose the pia with the use of microscissors. The surface of the brain was kept moist with the aid of physiological saline soaked gel foam (Pfizer, USA) throughout the experimental procedure.

To create a reference electrode, an 80 μm diameter teflon (PTFE)-coated PtIr wire (AM Systems, USA) was de-insulated 1–2 mm from one end. The deinsulated end was then placed in the subdural space. The wire was secured in place with gel foam (Pfizer, USA).

During the procedure, vitals were closely monitored (e.g. SPO_2, respiratory rate). To minimize the effects of brain pulsation, end-tidal CO_2 was typically maintained between 30–40 mmHg using mechanical ventilation. At the conclusion of the experimental procedures, animals were euthanized with an overdose of sodium pentobarbital (110 mg/kg, IV).

In-Vivo recordings

Electrophysiology system—Electrophysiology recordings were acquired using the Paradromics Argo System at a sampling frequency of 32 kHz. Typically for the recording procedure, isoflurane was reduced to <2% to reduce the effect of anesthesia on neural activity.

Rat Action Potential Recordings—Microwire arrays between 5 mm and 10 mm in diameter (n = 5) were implanted into the somatosensory and prefrontal regions of the rat cortex. These areas were targeted for the ease of insertion of the array into the rat cortex due to the limited brain size relative to the array diameter. A successfully inserted electrode typically had a peak-to-peak noise floor amplitude of 25–30 μV.

Spiking channels of interest were evaluated in real-time with the oscilloscope and strip chart modes on the UI to confirm the presence of spike-like waveforms (typical peak width < 1 ms). We also examined specific channels of interest to observe neural firing patterns and ensure that high frequency noise was not corrupting the signal.

As a final confirmation of that the signals recorded were physiological in origin, isoflurane levels were often increased to 5% at the end of the procedure to observe the loss of neural activity and the return of the channels to the 25–30 µV noise floor.

Auditory Paradigms—Auditory stimuli were presented free-field through multifield speakers (MF1, Tucker-Davis Technologies, USA) approximately 10 cm from the ear contralateral to the recording hemisphere. Signals were controlled using custom MATLAB software via a data acquisition system (USB-6366, National Instruments, USA) at a sampling rate of 192 kHz, which delivered the signal through an amplifier (SA1, Tucker-Davis Technologies, USA). The speaker was calibrated using a 0.25 inch condenser microphone (PCB Piezotronics,USA).

Pink noise was presented at 80 dB Sound Pressure Level (SPL) (100 ms duration with 10 ms rise/fall cos^2 ramp), with an inter-stimulus interval of 600 ms. For the rat, 800 stimuli were presented, and for the sheep, 500 stimuli were presented.

For the sheep, pure tones were also presented (50 ms duration with 10ms rise/fall cos^2 ramp) at levels from 40 to 80 dB SPL in 10 dB steps, at an inter-stimulus interval of 500 ms. Pure tones ranged from 0.5 to 32 kHz with 3 steps/octave, with 20 repetitions per stimulus.

Data export and backup—Immediately after each experiment, data were exported onto a portable solid-state drive (DC P4510, Intel, USA) and transferred to our server. This ensured redundancy in the event of data loss on the original recording system.

Offline Recording Analysis

Exported HDF5 files were imported into MATLAB. Channels were bandpass filtered (using the built-in 'filtfilt' function, forward and backward filtering to eliminate phase delays and distortions) from 300–6000 Hz. Channels were visually inspected, and their power spectra plotted, to confirm no noise source contamination. After initial data checks, spike sorting was performed on all the channels.

Spike sorting was performed using Wave_Clus [54]. Typical thresholds for neural data were set at least 3.5 times the noise threshold, calculated through Wave_Clus. In short, the noise threshold (σ) was calculated by taking the mean of the absolute value of the bandpassed signal and dividing it by 0.6745, and the spike crossing threshold was set at a minimum of 3.5σ [54]. The output of the batch processing was then used to confirm the presence or absence of spike waveforms. Single units were confirmed by three metrics: (1) all neural waveforms had a peak width less than 1 ms. (2) A neural interspike interval histogram [54,55] with a clear indication of a refractory period (i.e. no waveforms in the 0–3 ms bins on Wav_Clus output) was observed. (3) Clusters were clearly separated, as confirmed through the Wave_Clus user interface. Waveforms that did not match these criteria were deemed not to be single units and were not used for subsequent analysis.

Neural Activity Quality Metrics—To evaluate the recording quality of our isolated single units we calculated the peak-to-peak amplitude (P2P), noise, and signal-to-noise ratio (SNR). P2P was calculated by taking the peak-to-peak amplitude of median waveform of

the sorted putative single unit. The noise (StdNoise) was then determined by calculating the standard deviation of the RMS noise of the band-passed signal and multiplying it by two [38,56,57]. SNR was then calculated as P2P/StdNoise.

Sheep LFP recordings

Signal Conditioning—For LFP data analysis, all channels in the connectivity map generated immediately prior to the experiment were digitally band-pass filtered from 2 Hz to 400 Hz, with additional filtering to remove 60 Hz harmonics, and the resulting data were decimated to an effective sampling frequency of 1 kHz. To highlight evoked responses to pure tones stimuli in particular, and to further increase SNR for these recordings, the data were denoised by applying independent component analysis (ICA) [58]. The data were first scaled and whitened using principal component analysis, before performing ICA decomposition. Next, the data were further processed by applying the Hilbert transform and evoked responses were constructed from the envelope (2–400 Hz) of the signal amplitude to account for the oscillatory nature of the LFP waveforms.

Pink Noise Response Analysis—Evoked responses to pink noise were compared to baseline activity for each channel. The average baseline across trials was calculated using a time window of 100 ms preceding stimulus onset to stimulus onset, and the average response was determined using a window from 20 ms to 120 ms after stimulus onset. This additional 20 ms delay after stimulus onset was to accommodate for the minimum latency that we observed for auditory responses for surface LFP recordings, similar to that previously reported in other model systems [59–61]. The RMS was calculated by subtracting the RMS of the baseline window from the RMS of the signal in the response window. Channels having a RMS of greater than 10 μV were considered responding channels, and evoked responses for each channel were considered statistically significantly different from baseline activity if $p<0.05$, using a multiple comparisons permutation test [62].

Tone Response Analysis—Responses to each tone were averaged across trials and across all levels presented, since most responses were above threshold at the lowest presented level (i.e., 40 dB SPL). The non-parametric Wilcoxon Rank Sum tests with Bonferroni correction were used to distinguish statistically significant evoked responses from baseline ($p < 0.05$/number of channels), as the data were non-gaussian. A channel was considered responsive to pure tones if it had a statistically significant response to at least two tones (i.e., 0.6 octave bandwidth), and a RMS of at least 10 μV, which was considered the minimum response threshold. For these responding channels, the Best Frequency (BF) for each channel was determined as the tone which evoked the most significant response.

Results:

Here we designed and characterized the Argo system, which included a microwire electrode array of up to 31,000 channels bonded to a custom CMOS chip. Subsequent sections describe our characterization and validation of the system, which includes bench testing and performing *in vivo* experiments to record spikes in the rat cortex with 1300 microwires and surface LFP from the sheep auditory cortex with >30,000 microwires.

Benchtop characterization of the bonded microwire-electronics system

We validated the system through bench testing physiological saline by evaluating the connectivity between the microwires electrodes and the amplifier inputs on the CMOS-sensor. A summary of features and performance of the Argo can be seen in Table 1. Although electrodes at the periphery of the array occasionally showed lower connectivity, we were typically able to connect the majority of electrodes to an amplifier input using this process.

Connectivity tests were performed for every electrode array and sensor combination that was assembled. For 32 sensor/microwire array combinations, we obtained $71 \pm 2.9\%$ connectivity(+/−SEM) for all electrode pitches tested (60–300 μm).

The microelectrode array used for surface LFP recordings had an electrode pitch of 60 μm and the resulting 12 mm × 12 mm array contained ~35,000 electrodes. For this array, 30,146 pixels were connected to microwire electrodes, giving 86% connectivity (Figure 6A). The gain (+/− SD) was 811 ± 21 V/V, and the corresponding input-referred noise (+/−SD) was 6.3 ± 0.5 μV$_{RMS}$ in the 300 – 6000 Hz band (Figure 6B). From our k-means gain and noise analysis, 99.2% of the connected channels had < 10 μV$_{RMS}$ band-limited input-referred noise.

Across 32 CMOS sensor-bonded microwire arrays, the gain (+/− SD) was 763 ± 7 V/V, and the corresponding input-referred noise (+/−SD) was 7.5 ± 0.4 μV$_{RMS}$ in the 300 – 6000 Hz band. Thus, a large array of functional electrodes can be created using this CMOS sensor-microwire bonding approach with high connectivity across the sensor and good gain/noise characteristics for connected channels.

Rat Cortical Recordings

To validate our system *in vivo*, we show data from a 1300 microwire array (10 mm array diameter, 18 μm wire diameter, 200 μm spacing, 1 mm length), the highest channel count microwire array implanted into the rodent cortex to date. The array was implanted into the somatosensory and prefrontal regions of the rat cortex for ease of insertion of the large array due to these areas being on a flatter part of the rat cortex and requiring minimal rotational manipulation of the headstage for insertion. Together, this allowed for successful array insertion normal to the surface of the brain. Using this array, we were able to isolate 791 single units (Figure 7A,C). Mean +/− SEM peak-to-peak amplitude, noise and SNR values obtained across all units were 130 μV +/− 59.7, 10 μV +/− 2.2, 8.9 +/− 1.9 respectively (Supplementary Figure S1). Therefore, high fidelity neural activity can be recorded with the Argo recording system and associated microwire arrays along with a high unit count.

In addition to baseline recordings of spontaneous activity, pink noise auditory stimuli were presented to evoke somatosensory responses. Auditory stimuli were chosen in lieu of other sensory stimuli to avoid artifacts typically introduced by more direct somatosensory stimulation paradigms such as physical manipulation of the animal. We observed single units from somatosensory cortex that responded to auditory stimuli at an expected latency of 200 ms [63], further confirming neural activity (Figure 7D).

The rat cortex typically does not favor insertion of high density electrodes due to the brain size and high possibility of vascular insult [64–66] resulting in damage to neural tissue. However, we were able to obtain high fidelity recording with high unit count (Figure 6A,B) owing to our microwire design (electro-sharpening) and ease of insertion into the rat cortex.

Sheep Surface Recordings

While the rat cortex was ideal to validate the Argo system's ability to record neural action potentials, the size of the microwire array was limited by the small size of the rodent brain. As a result, recordings would always be limited to 1000–2000 electrodes, substantially smaller than the maximum channel count of the Argo system. We therefore developed microwire arrays for surface LFP recordings with over 30,000 connected channels in order to evaluate surface potentials from sheep cortex (n = 2). The ~30,000 channel limit was the result of a tradeoff between electrode spacing, ideal microwire diameter and recording site area to allow for the acquisition of surface LFP at an appropriate spatial resolution.

The microwire arrays used in these recordings had a pitch of 60 μm, with an overall array size of 12 mm × 12 mm. We targeted the array over the auditory cortex (centering at 25 mm lateral and 5 mm anterior of bregma). LFPs were recorded at the surface of the cortex in response to pink noise (Figure 8) as well as pure tones (Figure 9).

Prior to analysis, signals were conditioned using a series of infinite impulse response (IIR) notch resonators with Q factors > 25 at harmonics of 60 Hz within the frequency range under analysis to mitigate the effects of powerline noise [67–71]. The average noise contribution of 60 Hz harmonics in the 2–400 Hz range across the 30,146-channel array in a single recording file was 4.81 μV_{RMS}. Noise contributions from other recordings in this session were similar.

To quantify differences in evoked responses to pink noise compared to baseline activity, we first calculated the RMS for each channel in the 2 Hz to 400 Hz band (Figure 9A). As an initial measure of activation, we considered channels to be responsive if the evoked activity was at least 10 μV RMS higher than baseline, which is twice the determined noise floor. In one sheep, 21,963 channels of the 30,146 total channels (73%) showed an increase in power above threshold during the pink noise stimulus, with 16,412 (54%) of those channels' reponses being statistically significant. (Multiple comparisons nonparametric permutation test, $p < 0.05$) [62]. In a second sheep, we found that 17,233 of 31,239 total channels (55%) showed increased power, with 12,590 (40%) channels having a statistically significant response.

When presenting pure tone stimuli, we also observed frequency-specific responses (Figure 9), where 22,206 of 31,239 (71%) channels had at least 10 μV RMS activity above baseline and were significantly responsive to at least 2 tones (i.e., a minimum bandwidth of 0.6 octaves) (p < 0.05 Wilcoxon Rank Sum test, with Bonferroni correction). We then determined the BF for each channel by ranking the level of response to each frequency played. The BF for each channel was used to estimate the tonotopic organization across the cortex (Figure 9B). This was replicated in another experiment, where 26,054 of 30,146

(86%) channels were responsive, with a similar tonotopy across the cortex (Supplementary Figure S2).

Discussion:

Here we have described and characterized a neural recording system based on microwire electrodes compressively and reversibly bonded to a custom-designed CMOS amplifier array. We have demonstrated that these recording devices provide large gain and a low noise floor and can scale to a very large number of recording sites with optimal gain and noise distributions. This makes such devices suitable for massively parallel electrical recordings of spikes and LFP in animal cortex.

To validate this recording capability, we have demonstrated the largest microwire electrode array-based recordings in both rat and large animal cortex to date. We show the ability to record from over 30,000 channels simultaneously at full acquisition rates (32 kHz) in the sheep auditory cortex with good responses to auditory stimuli. Further, we show the ability to record high fidelity spikes in the rat cortex with our microwire based technology. Both results highlight and validate the capability to simultaneously record large channel count neural data at acquisition rates of 32 kHz with the Argo system.

Sheep Neural Recordings Demonstrate 30,000 channels of simultaneous acquisition

From the sheep cortex, we recorded surface LFP on over 30,000 channels with a 12 mm × 12 mm array, which is the largest neural recording in a large animal to date. Other studies from μECoG in large animals and humans range from 16–294 channels [73], therefore our system provides an order of magnitude increase in channel count. We performed surface LFP recordings using a high-density electrode array to mitigate the risk of damage to neurons that could have occurred upon insertion of a high-density penetrating array, resulting in poor recording quality.

The auditory cortex areas identified here were similar to those previously reported with histological tracing experiments in sheep [74,75], which reported the auditory cortex to be approximately 1 cm × 2 cm. Responses to auditory stimuli typically had a latency of approximately 20 ms after stimulus onset, which is expected with surface LFP recordings from other relevant animal models [59–61]. We did observe slightly different responses to tones across the microwire array between experiments, with one experiment revealing more channels with higher BFs. This is likely due to small differences in placement, especially since the array could span approximately half of the auditory cortex, and individual animal variation. Moreover, this tonotopy and sound-evoked responses were evident despite the acoustically noisy environment (i.e., an acute operating room setting rather than the traditional sound booth environment used in traditional auditory experiments), which could have led to increased variability in responses. However, even with this variation, we were able to find emerging tonotopy in the sheep auditory cortex.

Rat Neural Recordings Reveal High-fidelity Action Potentials

We demonstrate the ability to record from 791 single units in the rat cortex. This is significantly more than other microwire technology that has been used to record from

the rodent cortex, where the number of neurons ranges from 20–240 units in an acute setting [5,23,37,45,76,77]. We found the mean SNR across all channels to be close to 9, indicative of high fidelity recordings given that typical values using this metric define good SNR between 3 and 6 [35,38,56,78,79]. Here we demonstrate a system that is capable of producing low noise and high captured signal amplitude from single units. This is enabled in large part by the combination of tunable high pass and low pass filters that allow us to set the input bandwidth to reject both low and high frequency noise and remove aliasing effects.

Furthermore, the design of the microwires enables good performance for neural recordings. Specifically, our microwire electrodes have tip based recording sites, which are known to produce better recording quality compared to those sites that are along the length of the shaft, like some multi-depth silicon probes [3,57]. The electrosharpening of the tips also allows for ease of high-density array insertion into the brain [5,45] as has been demonstrated by our neural recordings, where we can successfully insert arrays into the rat cortex.

Future Recording Applications

Here we provide a demonstration for the utility of >30,000 channels for neural recording. The CMOS chip and data acquisition system is further capable of recording on all 65,536 channels simultaneously, provided a suitably large electrode array. Using 100% of the CMOS sensor would require an ordered electrode array for 1:1 bonding, unlike the disordered arrays used in the present study. The system can be modified to include interfacing ribbon cables that connect other electrode array types to the inputs of the CMOS chip [80–83]. Finally, the CMOS sensor could also be adapted to enable direct recording from the sensor input pads, which would serve as electrodes for recording from *in vitro* preparations of brain slices [84,85] or retinal explants [86].

Microwire-CMOS devices as Next Generation Brain-Computer Interfaces

Microwire-CMOS devices combine the robustness and longevity of traditional microwire electrodes with the advantages of active CMOS probes. Specifically, the design overcomes three of the greatest drawbacks of using microwire electrode arrays for neural recording. 1) By amplifying close to the signal source, the design reduces both input capacitance and noise pickup. 2) By providing on-chip multiplexing, the design allows for a much smaller number of lead wires and connectors than electrode sites. 3) Bonding pre-assembled arrays of microwires onto a CMOS sensor array provides a much simpler method of connecting the microwires than the traditional hand-wiring approach.

Here we demonstrate that microwire-CMOS is indeed scalable to tens of thousands of channels, but the current system is limited to acute, head-fixed preparations due to the size of the electronic components that lie downstream of the CMOS amplifier array. The clear next step is to develop a new ASIC and downstream architecture that are compatible with a floating microwire array configuration. Such a device would have a form factor similar to the Utah array but allow for greater electrode density, reduced tissue damage and insertion forces owing to smaller electrode diameter [5,36,45], and reduced interface cable thickness due to on-chip multiplexing of channels. Development of such a device is already underway.

Supplementary Material

Refer to Web version on PubMed Central for supplementary material.

Acknowledgments

References

[1]. Stevenson IH and Kording KP 2011 How advances in neural recording affect data analysis Nature Neuroscience 14 139–42 [PubMed: 21270781]

[2]. Stringer C, Pachitariu M, Steinmetz N, Reddy CB, Carandini M and Harris KD 2019 Spontaneous behaviors drive multidimensional, brainwide activity Science 364 255 [PubMed: 31000656]

[3]. Jun JJ, Steinmetz NA, Siegle JH, Denman DJ, Bauza M, Barbarits B, Lee AK, Anastassiou CA, Andrei A, Aydin Ç, Barbic M, Blanche TJ, Bonin V, Couto J, Dutta B, Gratiy SL, Gutnisky DA, Häusser M, Karsh B, Ledochowitsch P, Lopez CM, Mitelut C, Musa S, Okun M, Pachitariu M, Putzeys J, Rich PD, Rossant C, Sun W-L, Svoboda K, Carandini M, Harris KD, Koch C, O'Keefe J and Harris TD 2017 Fully integrated silicon probes for high-density recording of neural activity Nature 551 232–6 [PubMed: 29120427]

[4]. Musk E and Neuralink 2019 An Integrated Brain-Machine Interface Platform With Thousands of Channels J. Med. Internet Res. 21 e16194 [PubMed: 31642810]

[5]. Obaid A, Hanna M-E, Wu Y-W, Kollo M, Racz R, Angle MR, Müller J, Brackbill N, Wray W, Franke F, Chichilinsky EJ, Hierlemann A, Ding JB, Schaefer AT and Melosh NA 2020 Massively Parallel Microwire Arrays Integrated with CMOS chips for Neural Recording Science Advances

[6]. Dana H, Sun Y, Mohar B, Hulse BK, Kerlin AM, Hasseman JP, Tsegaye G, Tsang A, Wong A, Patel R, Macklin JJ, Chen Y, Konnerth A, Jayaraman V, Looger LL, Schreiter ER, Svoboda K and Kim DS 2019 High-performance calcium sensors for imaging activity in neuronal populations and microcompartments Nat. Methods 16 649–57 [PubMed: 31209382]

[7]. Chen T-W, Wardill TJ, Sun Y, Pulver SR, Renninger SL, Baohan A, Schreiter ER, Kerr RA, Orger MB, Jayaraman V, Looger LL, Svoboda K and Kim DS 2013 Ultrasensitive fluorescent proteins for imaging neuronal activity Nature 499 295–300 [PubMed: 23868258]

[8]. Piatkevich KD, Jung EE, Straub C, Linghu C, Park D, Suk H-J, Hochbaum DR, Goodwin D, Pnevmatikakis E, Pak N, Kawashima T, Yang C-T, Rhoades JL, Shemesh O, Asano S, Yoon Y-G, Freifeld L, Saulnier JL, Riegler C, Engert F, Hughes T, Drobizhev M, Szabo B, Ahrens MB, Flavell SW, Sabatini BL and Boyden ES 2018 A robotic multidimensional directed evolution approach applied to fluorescent voltage reporters Nat. Chem. Biol. 14 352–60 [PubMed: 29483642]

[9]. Hochbaum DR, Zhao Y, Farhi SL, Klapoetke N, Werley CA, Kapoor V, Zou P, Kralj JM, Maclaurin D, Smedemark-Margulies N, Saulnier JL, Boulting GL, Straub C, Cho YK, Melkonian M, Wong GK-S, Harrison DJ, Murthy VN, Sabatini BL, Boyden ES, Campbell RE and Cohen AE 2014 All-optical electrophysiology in mammalian neurons using engineered microbial rhodopsins Nat. Methods 11 825–33 [PubMed: 24952910]

[10]. Kozai TDY and Vazquez AL 2015 Photoelectric artefact from optogenetics and imaging on microelectrodes and bioelectronics: New Challenges and Opportunities J. Mater. Chem. B Mater. Biol. Med. 3 4965–78 [PubMed: 26167283]

[11]. Acker L, Pino EN, Boyden ES and Desimone R 2016 FEF inactivation with improved optogenetic methods Proc. Natl. Acad. Sci. U. S. A. 113 E7297–306 [PubMed: 27807140]

[12]. Strumwasser F 1958 Long-Term Recording from Single Neurons in Brain of Unrestrained Mammals Science 127 469–70 [PubMed: 13529005]

[13]. Hochberg LR, Bacher D, Jarosiewicz B, Masse NY, Simeral JD, Vogel J, Haddadin S, Liu J, Cash SS, van der Smagt P and Donoghue JP 2012 Reach and grasp by people with tetraplegia using a neurally controlled robotic arm Nature 485 372–5

[14]. Pandarinath C, Nuyujukian P, Blabe CH, Sorice BL, Saab J, Willett FR, Hochberg LR, Shenoy KV and Henderson JM 2017 High performance communication by people with paralysis using an intracortical brain-computer interface Elife 6

[15]. Hughes CL, Flesher SN, Weiss JM, Downey JE, Collinger JL and Gaunt RA Neural stimulation and recording performance in human somatosensory cortex over 1500 days

[16]. Lubin JA, Strebe JK and Kuo JS 2017 Intracortical Microstimulation of Human Somatosensory Cortex Reproduces Touch in Spinal Cord Injury Patient Neurosurgery 80 N29–30 [PubMed: 28586491]

[17]. Flesher SN, Collinger JL, Foldes ST, Weiss JM, Downey JE, Tyler-Kabara EC, Bensmaia SJ, Schwartz AB, Boninger ML and Gaunt RA 2016 Intracortical microstimulation of human somatosensory cortex Sci. Transl. Med. 8 361ra141

[18]. Misra A, Burke JF, Ramayya AG, Jacobs J, Sperling MR, Moxon KA, Kahana MJ, Evans JJ and Sharan AD 2014 Methods for implantation of micro-wire bundles and optimization of single/multi-unit recordings from human mesial temporal lobe Journal of Neural Engineering 11 026013 [PubMed: 24608589]

[19]. Cash SS and Hochberg LR 2015 The emergence of single neurons in clinical neurology Neuron 86 79–91 [PubMed: 25856488]

[20]. Truccolo W, Donoghue JA, Hochberg LR, Eskandar EN, Madsen JR, Anderson WS, Brown EN, Halgren E and Cash SS 2011 Single-neuron dynamics in human focal epilepsy Nat. Neurosci. 14 635–41 [PubMed: 21441925]

[21]. Rousche PJ and Normann RA 1998 Chronic recording capability of the Utah Intracortical Electrode Array in cat sensory cortex J. Neurosci. Methods 82 1–15 [PubMed: 10223510]

[22]. Willett FR, Avansino DT, Hochberg LR, Henderson JM and Shenoy KV High-performance brain-to-text communication via imagined handwriting

[23]. Chung JE, Joo HR, Fan JL, Liu DF, Barnett AH, Chen S, Geaghan-Breiner C, Karlsson MP, Karlsson M, Lee KY, Liang H, Magland JF, Pebbles JA, Tooker AC, Greengard LF, Tolosa VM and Frank LM 2019 High-Density, Long-Lasting, and Multi-region Electrophysiological Recordings Using Polymer Electrode Arrays Neuron 101 21–31.e5 [PubMed: 30502044]

[24]. Kozai TDY, Catt K, Li X, Gugel ZV, Olafsson VT, Vazquez AL and Cui XT 2015 Mechanical failure modes of chronically implanted planar silicon-based neural probes for laminar recording Biomaterials 37 25–39 [PubMed: 25453935]

[25]. Ceyssens F and Puers R 2015 Insulation lifetime improvement of polyimide thin film neural implants J. Neural Eng. 12 054001 [PubMed: 26269487]

[26]. van ara P, Boretius T, López-Álvarez VM, Maciejasz P, Andreu D, Raspopovic S, Petrini F M, Micera S, Granata G, Fernandez E, Rossini PM, Yoshida K, Jensen W, Divoux J-L, Guiraud D, Navarro X and Stieglitz T 2020 Stability of flexible thin-film metallization stimulation electrodes: analysis of explants after first-in-human study and improvement of in vivo performance J. Neural Eng.

[27]. Kollo M, Racz RR, Hanna M-ES, Obaid AM, Angle MR, Wray W, Kong Y, Hierlemann A, Müller J, Melosh NA and Schaefer AT CHIME: CMOS-hosted in-vivo microelectrodes for massively scalable neuronal recordings

[28]. McMahon DBT, Bondar IV, Afuwape OAT, Ide DC and Leopold DA 2014 One month in the life of a neuron: longitudinal single-unit electrophysiology in the monkey visual system J. Neurophysiol. 112 1748–62 [PubMed: 24966298]

[29]. Jackson A and Fetz EE 2007 Compact Movable Microwire Array for Long-Term Chronic Unit Recording in Cerebral Cortex of Primates Journal of Neurophysiology 98 3109–18 [PubMed: 17855584]

[30]. Nicolelis MAL, Dimitrov D, Carmena JM, Crist R, Lehew G, Kralik JD and Wise SP 2003 Chronic, multisite, multielectrode recordings in macaque monkeys Proc. Natl. Acad. Sci. U. S. A. 100 11041–6 [PubMed: 12960378]

[31]. Schwarz DA, Lebedev MA, Hanson TL, Dimitrov DF, Lehew G, Meloy J, Rajangam S, Subramanian V, Ifft PJ, Li Z, Ramakrishnan A, Tate A, Zhuang KZ and Nicolelis MAL 2014 Chronic, wireless recordings of large-scale brain activity in freely moving rhesus monkeys Nat. Methods 11 670–6 [PubMed: 24776634]

[32]. Hubel DH 1959 Single unit activity in striate cortex of unrestrained cats J. Physiol. 147 226–38 [PubMed: 14403678]

[33]. Hubel DH and Wiesel TN 1959 Receptive fields of single neurones in the cat's striate cortex The Journal of Physiology 148 574–91 [PubMed: 14403679]

[34]. Bartels J, Andreasen D, Ehirim P, Mao H, Seibert S, Wright EJ and Kennedy P 2008 Neurotrophic electrode: method of assembly and implantation into human motor speech cortex J. Neurosci. Methods 174 168–76 [PubMed: 18672003]

[35]. Kozai TDY, Langhals NB, Patel PR, Deng X, Zhang H, Smith KL, Lahann J, Kotov NA and Kipke DR 2012 Ultrasmall implantable composite microelectrodes with bioactive surfaces for chronic neural interfaces Nat. Mater. 11 1065–73 [PubMed: 23142839]

[36]. Patel PR, Na K, Zhang H, Kozai TDY, Kotov NA, Yoon E and Chestek CA 2015 Insertion of linear 8.4 µm diameter 16 channel carbon fiber electrode arrays for single unit recordings J. Neural Eng. 12 046009 [PubMed: 26035638]

[37]. Guitchounts G, Markowitz JE, Liberti WA and Gardner TJ 2013 A carbon-fiber electrode array for long-term neural recording J. Neural Eng. 10 046016 [PubMed: 23860226]

[38]. Sohal HS, Jackson A, Jackson R, Clowry GJ, Vassilevski K, O'Neill A and Baker SN 2014 The sinusoidal probe: a new approach to improve electrode longevity Front. Neuroeng 7 10 [PubMed: 24808859]

[39]. Khan A, Sahasrabuddhe K, Pouzzner D, Nishimura K and Angle M 2018 Data pipeline for 65,536 channels of extracellular unit recordings 40th Annual International Conference of the IEEE Engineering in Medicine and Biology Society (EMBC), Honolulu, HI, 2018, WeAT17.3.

[40]. Cogan SF 2008 Neural stimulation and recording electrodes Annu. Rev. Biomed. Eng. 10 275–309 [PubMed: 18429704]

[41]. Geddes LA and Roeder R 2003 Criteria for the selection of materials for implanted electrodes Ann. Biomed. Eng. 31 879–90 [PubMed: 12971619]

[42]. Musselman IH and Russell PE 1990 Platinum/iridium tips with controlled geometry for scanning tunneling microscopy J. Vac. Sci. Technol. A 8 3558–62

[43]. Chang W-T, Hwang I-S, Chang M-T, Lin C-Y, Hsu W-H and Hou J-L 2012 Method of electrochemical etching of tungsten tips with controllable profiles Rev. Sci. Instrum. 83 083704 [PubMed: 22938300]

[44]. Nordhausen Nordhausen, Rousche and Normann 1992 A Method For Acute Cerebral Cortex Recordings Using The Utah Intracortical Electrode Array Proceedings of the Annual International Conference of the IEEE Engineering in Medicine and Biology Society

[45]. Obaid A, Wu Y-W, Hanna M, Nix W, Ding J and Melosh N Ultra-sensitive measurement of brain penetration with microscale probes for brain machine interface considerations

[46]. Xie X, Rieth L, Williams L, Negi S, Bhandari R, Caldwell R, Sharma R, Tathireddy P and Solzbacher F 2014 Long-term reliability of Al2O3 and Parylene C bilayer encapsulated Utah electrode array based neural interfaces for chronic implantation J. Neural Eng. 11 026016 [PubMed: 24658358]

[47]. Randles JEB 1947 Kinetics of rapid electrode reactions Discuss. Faraday Soc. 1 11–9

[48]. Sankar V, Patrick E, Dieme R, Sanchez JC, Prasad A and Nishida T 2014 Electrode impedance analysis of chronic tungsten microwire neural implants: understanding abiotic vs. biotic contributions Frontiers in Neuroengineering 7

[49]. Mercanzini A, Colin P, Bensadoun J-C, Bertsch A and Renaud P 2009 In vivo electrical impedance spectroscopy of tissue reaction to microelectrode arrays IEEE Trans. Biomed. Eng. 56 1909–18

[50]. Straka MM, Shafer B, Vasudevan S, Welle C and Rieth L 2018 Characterizing Longitudinal Changes in the Impedance Spectra of In-Vivo Peripheral Nerve Electrodes Micromachines (Basel) 9

[51]. Lewicki MS 1998 A review of methods for spike sorting: the detection and classification of neural action potentials Network: Computation in Neural Systems 9 R53–78

[52]. Ghanbari Y, Papamichalis P and Spence L 2009 Robustness of neural spike sorting to sampling rate and quantization bit depth 2009 16th International Conference on Digital Signal Processing

[53]. Ludwig KA, Miriani RM, Langhals NB, Joseph MD, Anderson DJ and Kipke DR 2009 Using a common average reference to improve cortical neuron recordings from microelectrode arrays J. Neurophysiol. 101 1679–89 [PubMed: 19109453]

[54]. Quiroga RQ, Nadasdy Z and Ben-Shaul Y 2004 Unsupervised spike detection and sorting with wavelets and superparamagnetic clustering Neural Comput. 16 1661–87 [PubMed: 15228749]

[55]. Rossant C, Kadir SN, Goodman DFM, Schulman J, Hunter MLD, Saleem AB, Grosmark A, Belluscio M, Denfield GH, Ecker A S, Tolias AS, Solomon S, Buzsaki G, Carandini M and Harris KD 2016 Spike sorting for large, dense electrode arrays Nat. Neurosci. 19 634–41 [PubMed: 26974951]

[56]. Ludwig KA, Langhals NB, Joseph MD, Richardson-Burns SM, Hendricks JL and Kipke DR 2011 Poly(3,4-ethylenedioxythiophene) (PEDOT) polymer coatings facilitate smaller neural recording electrodes J. Neural Eng. 8 014001 [PubMed: 21245527]

[57]. Kipke DR, Vetter RJ, Williams JC and Hetke JF 2003 Silicon-substrate intracortical microelectrode arrays for long-term recording of neuronal spike activity in cerebral cortex IEEE Trans. Neural Syst. Rehabil. Eng. 11 151–5 [PubMed: 12899260]

[58]. Hyvärinen A and Oja E 2000 Independent component analysis: algorithms and applications Neural Netw. 13 411–30 [PubMed: 10946390]

[59]. Kajikawa Y and Schroeder CE 2011 How local is the local field potential? Neuron 72 847–58 [PubMed: 22153379]

[60]. Escabí MA, Read HL, Viventi J, Kim D-H, Higgins NC, Storace DA, Liu ASK, Gifford AM, Burke JF, Campisi M, Kim Y-S, Avrin AE, der Spiegel Jan V, Huang Y, Li M, Wu J, Rogers JA, Litt B and Cohen YE 2014 A high-density, high-channel count, multiplexed μECoG array for auditory-cortex recordings J. Neurophysiol. 112 1566–83 [PubMed: 24920021]

[61]. Trumpis M, Insanally M, Zou J, Elsharif A, Ghomashchi A, Sertac Artan N, Froemke RC and Viventi J 2017 A low-cost, scalable, current-sensing digital headstage for high channel count μECoG J. Neural Eng. 14 026009 [PubMed: 28102827]

[62]. Nichols TE and Holmes AP 2002 Nonparametric permutation tests for functional neuroimaging: a primer with examples Hum. Brain Mapp. 15 1–25 [PubMed: 11747097]

[63]. Maruyama AT and Komai S 2018 Auditory-induced response in the primary sensory cortex of rodents PLoS One 13 e0209266 [PubMed: 30571722]

[64]. Blinder P, Tsai PS, Kaufhold JP, Knutsen PM, Suhl H and Kleinfeld D 2013 The cortical angiome: an interconnected vascular network with noncolumnar patterns of blood flow Nat. Neurosci. 16 889–97 [PubMed: 23749145]

[65]. Kozai TDY, Marzullo TC, Hooi F, Langhals NB, Majewska AK, Brown EB and Kipke DR 2010 Reduction of neurovascular damage resulting from microelectrode insertion into the cerebral cortex using in vivo two-photon mapping J. Neural Eng. 7 046011 [PubMed: 20644246]

[66]. He F, Sullender C, Zhu H, Williamson MR, Li X, Zhao Z, Jones TA, Xie C, Dunn AK and Luan L Multimodal mapping of neural activity and cerebral blood flow reveals long-lasting neurovascular dissociations after small-scale strokes

[67]. Herff SA, Herff C, Milne AJ, Johnson GD, Shih JJ and Krusienski DJ 2020 Prefrontal High Gamma in ECoG Tags Periodicity of Musical Rhythms in Perception and Imagination eNeuro 7

[68]. Jiang T, Pellizzer G, Asman P, Bastos D, Bhavsar S, Tummala S, Prabhu S and Ince NF 2020 Power Modulations of ECoG Alpha/Beta and Gamma Bands Correlate With Time-Derivative of Force During Hand Grasp Front. Neurosci. 14 100 [PubMed: 32116533]

[69]. Ahmadipour P, Yang Y, Chang EF and Shanechi MM 2020 Adaptive tracking of human ECoG network dynamics Journal of Neural Engineering

[70]. Luck SJ 2014 An introduction to the event-related potential technique. 2nd Cambridge. [Google Scholar]

[71]. David SV, Malaval N and Shamma SA 2010 Decoupling action potential bias from cortical local field potentials Comput. Intell. Neurosci 393019 [PubMed: 20169096]

[72]. Gierthmuehlen M, Wang X, Gkogkidis A, Henle C, Fischer J, Fehrenbacher T, Kohler F, Raab M, Mader I, Kuehn C, Foerster K, Haberstroh J, Freiman TM, Stieglitz T, Rickert J, Schuettler M and Ball T 2014 Mapping of sheep sensory cortex with a novel microelectrocorticography grid J. Comp. Neurol. 522 3590–608 [PubMed: 24851798]

[73]. Chiang C-H, Lee J, Wang C, Williams AJ, Lucas TH, Cohen YE and Viventi J 2020 A modular high-density µECoG system on macaque vlPFC for auditory cognitive decoding J. Neural Eng.

[74]. Gierthmuehlen M, Wang X, Gkogkidis A, Henle C, Fischer J, Fehrenbacher T, Kohler F, Raab M, Mader I, Kuehn C, Foerster K, Haberstroh J, Freiman TM, Stieglitz T, Rickert J, Schuettler M and Ball T 2014 Mapping of sheep sensory cortex with a novel microelectrocorticography grid J. Comp. Neurol. 522 3590–608 [PubMed: 24851798]

[75]. Michaloudi H, Karamanlidis AN, Dinopoulos A, Papadopoulos G and Antonopoulos J 1986 Thalamic projections to the posterior sylvian and posterior ectosylvian gyri of the sheep brain, revealed with the retrograde transport of horseradish peroxidase Anat. Embryol. 175 77–90

[76]. Massey TL, Santacruz SR, Hou JF, Pister KSJ, Carmena JM and Maharbiz MM 2019 A high-density carbon fiber neural recording array technology J. Neural Eng. 16 016024 [PubMed: 30524060]

[77]. Pfeiffer BE and Foster DJ 2013 Hippocampal place-cell sequences depict future paths to remembered goals Nature 497 74–9 [PubMed: 23594744]

[78]. Ward MP, Rajdev P, Ellison C and Irazoqui PP 2009 Toward a comparison of microelectrodes for acute and chronic recordings Brain Res. 1282 183–200 [PubMed: 19486899]

[79]. Xu H, Hirschberg AW, Scholten K, Berger TW, Song D and Meng E 2018 Acute in vivo testing of a conformal polymer microelectrode array for multi-region hippocampal recordings J. Neural Eng. 15 016017 [PubMed: 29044049]

[80]. Wise KD, Sodagar AM, Yao Y, Gulari MN, Perlin GE and Najafi K 2008 Microelectrodes, Microelectronics, and Implantable Neural Microsystems Proc. IEEE 96 1184–202

[81]. Perlin GE and Wise KD 2010 An Ultra Compact Integrated Front End for Wireless Neural Recording Microsystems J. Microelectromech. Syst. 19 1409–21

[82]. Merriam ME, Dehmel S, Srivannavit O, Shore SE and Wise KD 2011 A 3-d 160-site microelectrode array for cochlear nucleus mapping IEEE Trans. Biomed. Eng. 58 397–403 [PubMed: 20959259]

[83]. Ruther P and Paul O 2015 New approaches for CMOS-based devices for large-scale neural recording Curr. Opin. Neurobiol. 32 31–7 [PubMed: 25463562]

[84]. Hormuzdi SG, Pais I, LeBeau FE, Towers SK, Rozov A, Buhl EH, Whittington MA and Monyer H 2001 Impaired electrical signaling disrupts gamma frequency oscillations in connexin 36-deficient mice Neuron 31 487–95 [PubMed: 11516404]

[85]. Florez CM, McGinn RJ, Lukankin V, Marwa I, Sugumar S, Dian J, Hazrati L N, Carlen PL, Zhang L and Valiante TA 2015 In vitro recordings of human neocortical oscillations Cereb. Cortex 25 578–97

[86]. Tsai D, Sawyer D, Bradd A, Yuste R and Shepard KL 2017 A very large-scale microelectrode array for cellular-resolution electrophysiology Nat. Commun. 8 1802 [PubMed: 29176752]
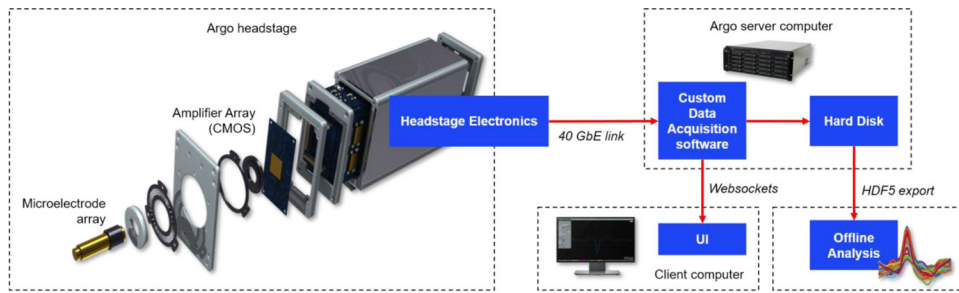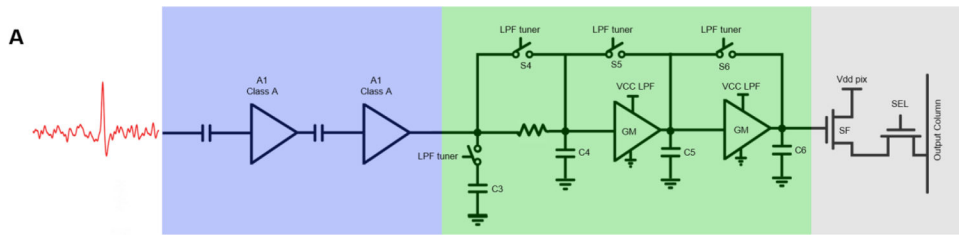
Figure 1:

Block diagram of the Argo System. The Argo headstage comprises recording electrodes, the CMOS amplifier array, and electronics to digitize, packetize, and transmit signals over the optical data link. This data link connects it to the recording server computer, which hosts custom data acquisition software and a User Interface server. A client computer is used to read data from the server and display it in the system user interface. Data are exported as HDF5 files from the server and read into an offline processing computer where analysis and spike sorting are performed.
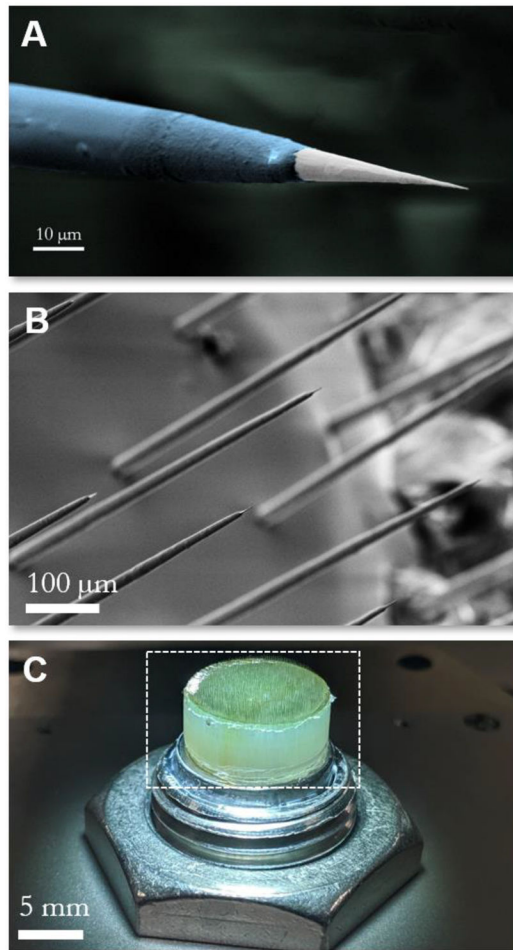
Figure 2: Microwire recording electrodes.

(A) False color electron micrograph of a single electrosharpened microwire showing taper along the electrode length, alumina insulation layer (blue) and recording site at the tip (white), and (B) micrograph of the distal end of the microwire array showing a field of electrodes with electrosharpened tips. (C) Macroscopic optical image of the electrode array, highlighting the etched back recording end (white dashed box).

Figure 3: CMOS sensor characterization.

The input signal is AC-coupled into two common-source amplifiers biased in the Class A configuration (A1, A2, shown in blue), which together form the front-end low noise amplifier (LNA) chain. Each stage has a gain of 10 V/V. The third stage (green) is a third-order tunable low-pass filter that serves as an anti-aliasing filter. The final stages (grey) are for pixel selection to read out the stored value.
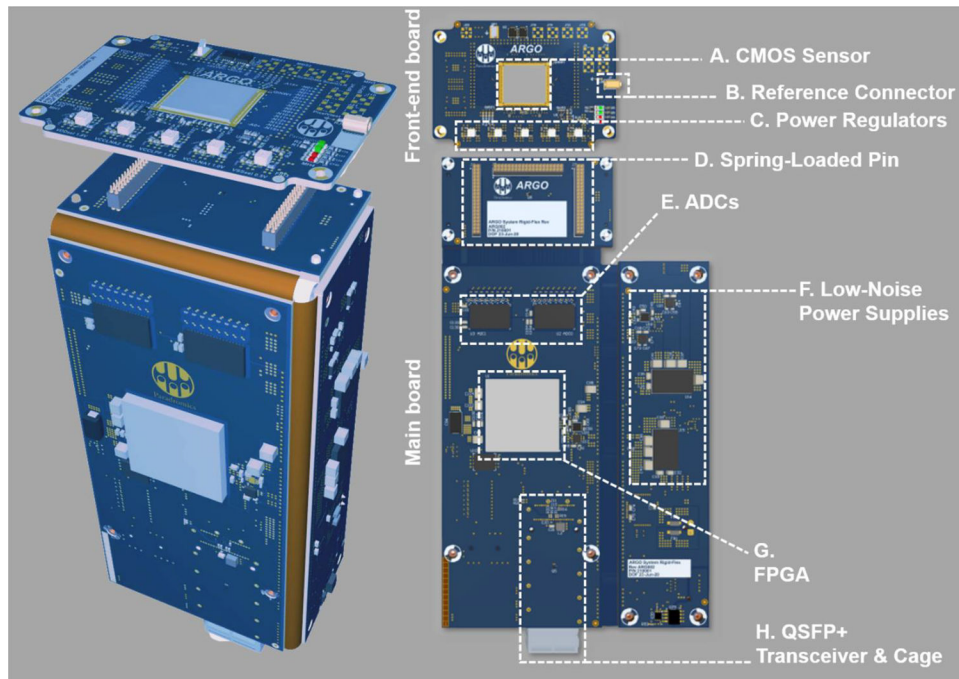
Figure 4: System electronics.

The Argo system's electronics are housed on two custom PCBs. (Left) PCBs are folded and aligned to fit the metal housing of the Argo system. (Right) A smaller PCB (the front-end board) holds the CMOS sensor (A), reference connector (B), and power regulators (C) for the sensor. This front-end board is connected to a larger main board via three banks of spring-loaded connectors (D). On this main board sit the analog-to-digital converters (ADCs, E), low-noise power supplies (F), the FPGA (G), and the Quad Small Form-factor Pluggable (QSFP+) transceiver and connector (H) over which data are transmitted using an optical fiber (not pictured).
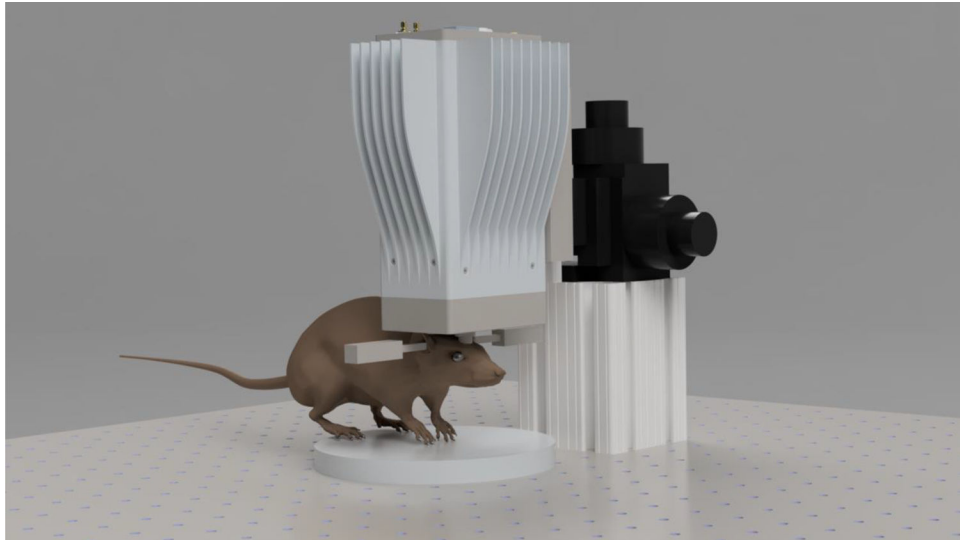
Figure 5: Schematic of the experimental setup of acute, head-fixed *in-vivo* experiments.
The Argo system is mounted to a three-axis stage that translates the system longitudinally, laterally, and vertically to position and insert the array into the brain of a head-fixed animal (rat pictured). The head is held in a stereotaxic frame (not shown) with ear bars (pictured on either side of the animal's head). The stages used for sheep experiments were larger to accommodate the travel required to position the array over the craniotomy in the larger head.
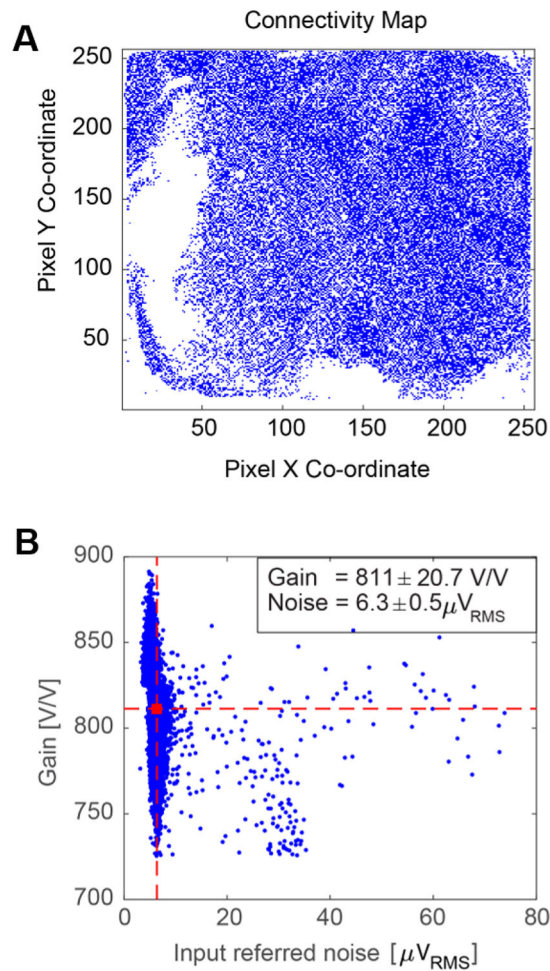
Figure 6: Full signal chain characterization in saline bath prior to *in vivo* experiment.
(A) Raster image of the full sensor showing pixels connected to active electrodes for an array of approx. 35,000 electrodes. (B) Gain and noise distribution for the connected pixels. Channel clusters with mean gain >650V/V and mean noise <10 μV_{RMS} were selected for further analysis; here, the mean gain was 811 V/V (horizontal dashed red line), and the mean noise was 6.5 μV_{RMS} (vertical dashed red line). The final connectivity map contained 30,146 channels for analysis, resulting in a connectivity of 86%.
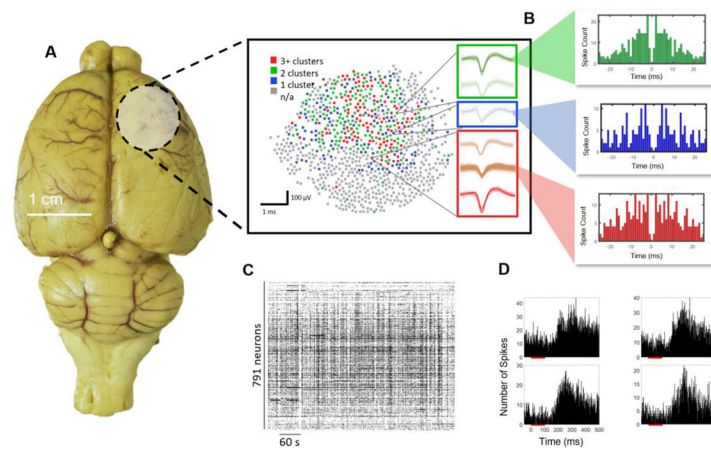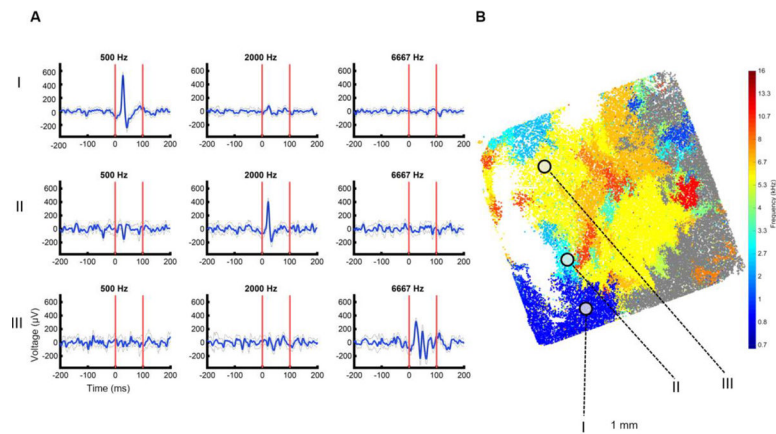
Figure 7.
Rat cortex spike recordings. (A) Distribution of units found over the implantation of 1300 microwires in the rat cortex. The circular shaded region shows the location of the craniotomy and the brain region that was implanted, and the map shows channels with 0–3+ spike clusters. (B) Example autocorrelogram from specific highlighted units, showing the emergence of well isolated single units. (C) A total of 791 single units as shown by the spike raster were found in the recording with good temporal dynamics associated with neuronal firing under anesthesia. (D) Example post-stimulus time histograms responses of single units in the somatosensory cortex to auditory pink noise stimuli (red bar). A latency of around 200 ms is observed, as expected from somatosensory neurons responding to auditory stimuli [63].
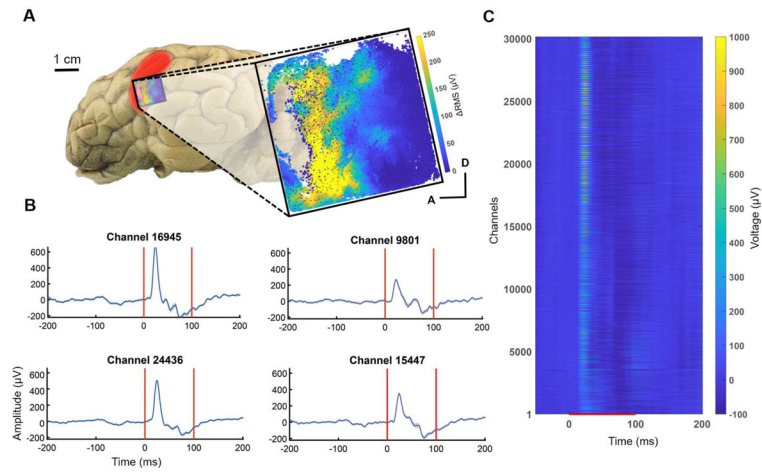
Figure 8.
Pink noise evoked potentials across the 30,000-channel microwire array from the sheep auditory cortex (red shaded area, described in [72]). (A) Location of the array (blue shaded boundary) for the auditory cortex surface recording and a map of RMS (i.e., response RMS minus baseline RMS) for individual channels in response to pink noise. With the RMS of at least 10 µV, 21,963 of these channels were responders to pink noise, A (anterior) and D (dorsal) for the channel location in the array. (B) Evoked potentials (mean +/− SEM) from representative responding electrodes. (C) Trial-averaged evoked potentials of all 30,146 channels in response to pink noise. The red line denotes when the stimulus was presented. Channels were ordered spatially by the pixel location.

Figure 9.
Frequency specific responses with emerging tonotopic organization for the sheep auditory cortex. (A) Evoked potentials from electrodes across the microwire array demarcated from (I-III) are characteristic of frequency specific responses. (B) Array map with electrodes color coded for BF. Non-significantly responding electrodes shown in gray (Wilcoxon rank-sum, $p < 0.05$, Bonferroni corrected).

Table 1:

A Summary of Key Features and Performance of the Argo System

Parameter	Specification
No. of neural sensors	Up to 65,536 (256 × 256)
Amplifier pixel size	50 μm x 50 μm
Electrosharpened Electrode Impedance	300 – 500 kΩ
CMOS/microwire array connectivity	71 ± 2.9% (SEM)
Gain for CMOS sensor-bonded arrays (n=32)	763 ± 7 V/V (SD)
Input referred noise for CMOS sensor-bonded arrays (n=32)	6.3 ± 0.5 μV$_{RMS}$ (SD)
Full-frame readout to disk	Up to 39,000 frames per second
Continuous recording time	>8 hours